Exact Diagonalization Techniques

Chapter *in* Lecture Notes in Physics · December 2007

DOI: 10.1007/978-3-540-74686-7_18

CITATIONS
40

READS
3,162

2 authors, including:

H. Fehske
University of Greifswald
442 PUBLICATIONS **7,399** CITATIONS

SEE PROFILE

18 Exact Diagonalization Techniques

Alexander Weiße and Holger Fehske

Institut für Physik, Universität Greifswald, 17487 Greifswald, Germany

In this chapter we show how to calculate a few eigenstates of the full Hamiltonian matrix of an interacting quantum system. Naturally, this implies that the Hilbert space of the problem has to be truncated, either by considering finite systems or by imposing suitable cut-offs, or both. All of the presented methods are iterative, i.e., the Hamiltonian matrix is applied repeatedly to a set of vectors from the Hilbert space. In addition, most quantum many-particle problems lead to a sparse matrix representation of the Hamiltonian, where only a very small fraction of the matrix elements is non-zero.

18.1 Basis Construction

18.1.1 Typical Quantum Many-Particle Models

Before we can start applying sparse matrix algorithms, we need to translate the considered many-particle Hamiltonian, given in the language of second quantization, into a sparse Hermitian matrix. Usually, this is the intellectually and technically challenging part of the project, in particular, if we want to take into account symmetries of the problem.

Typical lattice models in solid state physics involve electrons, spins and phonons. Within this part we will focus on the Hubbard model,

$$H = -t \sum_{\langle ij \rangle, \sigma} \left(c^\dagger_{i\sigma} c_{j\sigma} + \text{H.c.} \right) + U \sum_i n_{i\uparrow} n_{i\downarrow} \ , \tag{18.1}$$

which describes a single band of electrons $c^{(\dagger)}_{i\sigma}$ ($n_{i\sigma} = c^\dagger_{i\sigma} c_{i\sigma}$) with on-site Coulomb interaction U. Originally [1, 2, 3], it was introduced to study correlation effects and ferromagnetism in narrow band transition metals. After the discovery of high-T_C superconductors the model became very popular again, since it is considered as the simplest lattice model which, in two dimensions, may have a superconducting phase. In one dimension, the model is exactly solvable [4, 5], hence we can check our numerics for correctness. From the Hubbard model at half-filling, taking the limit $U \to \infty$, we can derive the Heisenberg model

$$H = \sum_{ij} J_{ij} \, \boldsymbol{S}_i \cdot \boldsymbol{S}_j \ , \tag{18.2}$$

A. Weiße and H. Fehske: *Exact Diagonalization Techniques*, Lect. Notes Phys. **739**, 529–544 (2008)
DOI 10.1007/978-3-540-74686-7_18

which accounts for the magnetic properties of insulating compounds that are governed by the exchange interaction $J \sim t^2/U$ between localized spins $\boldsymbol{S}_i$. In many solids the electronic degrees of freedom will interact also with vibrations of the crystal lattice, described in harmonic approximation by bosons $b_i^{(\dagger)}$ (phonons). This leads to microscopic models like the Holstein-Hubbard model

$$\begin{aligned} H = &- t \sum_{\langle ij\rangle,\sigma} (c_{i\sigma}^\dagger c_{j\sigma} + \text{H.c.}) + U \sum_i n_{i\uparrow} n_{i\downarrow} \\ &- g\omega_0 \sum_{i,\sigma} (b_i^\dagger + b_i) n_{i\sigma} + \omega_0 \sum_i b_i^\dagger b_i \; . \end{aligned} \tag{18.3}$$

With the methods described in this part, such models can be studied on finite clusters with a few dozen sites, both at zero and at finite temperature. In special cases, e.g., for the problem of few polarons, also infinite systems are accessible.

18.1.2 The Hubbard Model and its Symmetries

To be specific, let us derive all the general concepts of basis construction for the Hubbard model on an one-dimensional chain or ring. For a single site i, the Hilbert space of the model (18.1) consists of four states,

(i) $|0\rangle$ = no electron at site i,
(ii) $c_{i\downarrow}^\dagger|0\rangle$ = one down-spin electron at site i,
(iii) $c_{i\uparrow}^\dagger|0\rangle$ = one up-spin electron at site i, and
(iv) $c_{i\uparrow}^\dagger c_{i\downarrow}^\dagger|0\rangle$ = two electrons at site i.

Consequently, for a finite cluster of L sites, the full Hilbert space has dimension 4^L. This is a rapidly growing number, and without symmetrization we could not go beyond $L \approx 16$ even on the biggest supercomputers.

Given a symmetry of the system, i.e. an operator A that commutes with H, the Hamiltonian will not mix states from different eigenspaces of A. Therefore, the matrix representing H will acquire a block structure, and we can handle each block separately (see Fig. 18.1). The Hubbard Hamiltonian (18.1) has a number of symmetries:

– Particle number conservation: H commutes with total particle number

$$N_\text{e} = \sum_{i,\sigma} n_{i\sigma} \; . \tag{18.4}$$

– $SU(2)$ spin symmetry: H commutes with all components of the total spin

$$S^\alpha = \frac{1}{2} \sum_i \sum_{\mu,\nu} c_{i\mu}^\dagger \sigma_{\mu\nu}^\alpha c_{i\nu} \; , \tag{18.5}$$

where σ^α denotes the Pauli matrices, and $\mu, \nu \in \{\uparrow, \downarrow\}$.

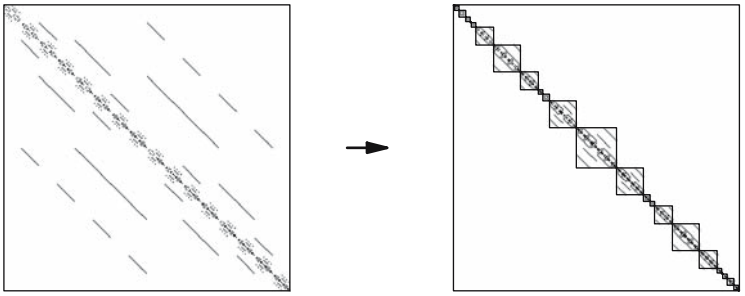

Fig. 18.1. With the use of symmetries the Hamiltonian matrix acquires a block structure. Here: The matrix for the Hubbard model when particle number conservation is neglected (**left**) or taken into account (**right**)

– Particle-hole symmetry: For an even number of lattice sites H is invariant under the transformation

$$Q: \; c_{i,\sigma} \to (-1)^i c^\dagger_{i,-\sigma} \; , \qquad c^\dagger_{i,\sigma} \to (-1)^i c_{i,-\sigma} \; , \tag{18.6}$$

except for a constant.

– Translational invariance: Assuming periodic boundary conditions, i.e., $c^{(\dagger)}_{L,\sigma} = c^{(\dagger)}_{0,\sigma}$, H commutes with the translation operator

$$T: \; c^{(\dagger)}_{i,\sigma} \to c^{(\dagger)}_{i+1,\sigma} \; . \tag{18.7}$$

Here L is the number of lattice sites.

– Inversion symmetry: H is symmetric with respect to the inversion

$$I: \; c^{(\dagger)}_{i,\sigma} \to c^{(\dagger)}_{L-i,\sigma} \; . \tag{18.8}$$

For the basis construction the most important of these symmetries are the particle number conservation, the spin-S^z conservation and the translational invariance. Note that the conservation of both $S^z = (N_\uparrow - N_\downarrow)/2$ and $N_\mathrm{e} = N_\uparrow + N_\downarrow$ is equivalent to the conservation of the total number of spin-$\uparrow$ and of spin-$\downarrow$ electrons, $N_\uparrow$ and $N_\downarrow$, respectively. In addition to S^z we could also fix the total spin S^2, but the construction of the corresponding eigenstates is too complicated for most practical computations.

18.1.3 A Basis for the Hubbard Model

Let us start with building the basis for a system with L sites and fixed electron numbers $N_\uparrow$ and $N_\downarrow$. Each element of the basis can be identified by the positions of the up and down electrons, but for uniqueness we also need to define some normal

order. For the Hubbard model it is convenient to first sort the electrons by the spin index, then by the lattice index, i.e.,

$$c^\dagger_{3\uparrow} c^\dagger_{2\uparrow} c^\dagger_{0\uparrow} c^\dagger_{3\downarrow} c^\dagger_{1\downarrow} |0\rangle \tag{18.9}$$

is a valid ordered state. This ordering has the advantage that the nearest-neighbor hopping in the Hamiltonian does not lead to complicated phase factors, when applied to our basis states. Finding all the basis states is a combinatorics problem: There are $\binom{L}{N_\uparrow}$ ways of distributing $N_\uparrow$ (indistinguishable) up-spin electrons on L sites, and similarly, $\binom{L}{N_\downarrow}$ ways of distributing $N_\downarrow$ down-spin electrons on L sites. Hence, the total number of states in our basis is $\binom{L}{N_\uparrow}\binom{L}{N_\downarrow}$. If we sum up the dimensions of all $(N_\uparrow, N_\downarrow)$-blocks, we obtain

$$\sum_{N_\uparrow=0}^{L} \sum_{N_\downarrow=0}^{L} \binom{L}{N_\uparrow}\binom{L}{N_\downarrow} = 2^L 2^L = 4^L \,, \tag{18.10}$$

which is the total Hilbert space dimension we derived earlier. The biggest block in our symmetrized Hamiltonian has $N_\uparrow = N_\downarrow = L/2$ and dimension $\binom{L}{L/2}^2$. This is roughly a factor of $\pi L/2$ smaller than the original 4^L. Below we will reduce the dimension of the biggest block by another factor of L using translational invariance.

Knowing the basic structure and the dimension of the Hilbert space with fixed particle numbers, how can we implement it on a computer? An efficient way to do so, is using integer numbers and bit operations that are available in many programming languages. Assume, we work with a lattice of $L = 4$ sites and $N_\uparrow = 3$, $N_\downarrow = 2$. We can then translate the state of (18.9) into a bit pattern,

$$c^\dagger_{3\uparrow} c^\dagger_{2\uparrow} c^\dagger_{0\uparrow} c^\dagger_{3\downarrow} c^\dagger_{1\downarrow} |0\rangle \rightarrow (\uparrow, \uparrow, 0, \uparrow) \times (\downarrow, 0, \downarrow, 0) \rightarrow 1101 \times 1010 \,. \tag{18.11}$$

To build the other basis states, we need all four-bit integers with three bits set to one, as well as all four-bit integers with two bits set. We leave this to the reader as a little programming exercise, and just quote the result in Table 18.1.

The complete basis is given by all 24 pairs of the four up-spin and the six down-spin states. Having ordered the bit patterns by the integer values they correspond to,

Table 18.1. Basis states of the Hubbard model on four sites with three up- and two down-spin electrons

no.	$\uparrow$-patterns	no.	$\downarrow$-patterns
0	0111 = 7	0	0011 = 3
1	1011 = 11	1	0101 = 5
2	1101 = 13	2	0110 = 6
3	1110 = 14	3	1001 = 9
		4	1010 = 10
		5	1100 = 12

we can label each state by its indices (i, j) in the list of up and down patterns, or combine the two indices to an overall index $n = i \cdot 6 + j$. Our sample state (18.9) corresponds to the index pair $(2, 4)$, which is equivalent to the state $2 \cdot 6 + 4 = 16$ of the total 24 states.

18.1.4 The Hamiltonian Matrix

Having found all basis states, we can now apply the Hamiltonian (18.1) to each of them, to obtain the matrix elements. The hopping term corresponds to the left or right shift of single bits. For periodic boundary conditions we need to take care of potential minus signs, whenever an electron is wrapped around the boundary and the number of electrons it commutes through is odd. The Coulomb interaction merely counts double occupancy, i.e. bits which are set in both the up and down spin part of the basis state. For our sample state (18.9) we obtain:

$$\begin{aligned}
\uparrow\text{-hopping}: &\ 1101 \times 1010 \rightarrow -t\,(1011 + 1110) \times 1010\ , \\
\downarrow\text{-hopping}: &\ 1101 \times 1010 \rightarrow -t\,1101 \times (0110 + 1100 + 1001 - 0011)\ , \\
U\text{-term}: &\ 1101 \times 1010 \rightarrow U\,1101 \times 1010\ .
\end{aligned} \tag{18.12}$$

Now we need to find the indices of the resulting states on the right. For the Hubbard model with its decomposition into two spin channels, we can simply use a table which translates the integer value of the bit pattern into the index in the list of up and down spin states (see Table 18.1). Note, however, that this table has a length of 2^L. When simulating spin or phonon models such a table would easily exceed all available memory. For finding the index of a given basis state we then need to resort to other approaches, like hashing, fast search algorithms or some decomposition of the state [6]. Having found the indices and denoting our basis in a ket-notation, $|n\rangle$, (18.12) reads

$$\begin{aligned}
\uparrow\text{-hopping}: &\quad |16\rangle \rightarrow -t\,(|10\rangle + |22\rangle)\ , \\
\downarrow\text{-hopping}: &\quad |16\rangle \rightarrow -t\,(|14\rangle + |17\rangle + |15\rangle - |12\rangle)\ , \\
U\text{-term}: &\quad |16\rangle \rightarrow U\,|16\rangle\ .
\end{aligned} \tag{18.13}$$

To obtain the complete Hamiltonian matrix we have to repeat this procedure for all 24 basis states. In each case we obtain a maximum of $2L = 8$ off-diagonal non-zero matrix elements. Thus, the matrix is indeed very sparse (see Fig. 18.2). The generalization of the above considerations to arbitrary values of L, $N_\uparrow$, and $N_\downarrow$ is straight-forward. For spatial dimensions larger than one we need to be a bit more careful with fermionic phase factors. In general, minus signs will occur not only at the boundaries, but also for other hopping processes.

18.1.5 Using Translation Symmetry

We mentioned earlier that the translation symmetry of the Hubbard model (or any other lattice model) can be used for a further reduction of the Hilbert space dimension. What we need are the eigenstates of the translation operator T, which can be

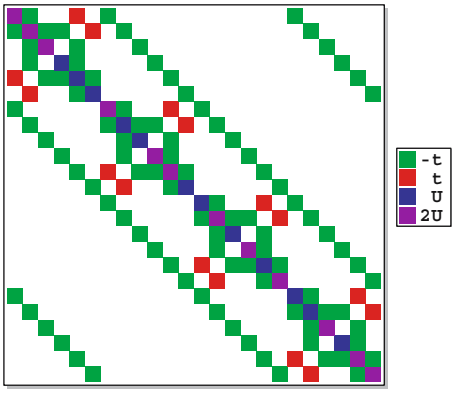

Fig. 18.2. Schematic representation of the Hamiltonian matrix of the Hubbard model with $L = 4$, $N_\uparrow = 3$, $N_\downarrow = 2$, and periodic boundary conditions

constructed using the projector

$$P_k = \frac{1}{L} \sum_{j=0}^{L-1} \mathrm{e}^{2\pi \mathrm{i} jk/L} T^j \; . \tag{18.14}$$

Clearly, for a given (unsymmetrized) state $|n\rangle$, the state $P_k|n\rangle$ is an eigenstate of T,

$$T P_k|n\rangle = \frac{1}{L} \sum_{j=0}^{L-1} \mathrm{e}^{2\pi \mathrm{i} jk/L} T^{j+1}|n\rangle = \mathrm{e}^{-2\pi \mathrm{i} k/L} P_k|n\rangle \; , \tag{18.15}$$

where the corresponding eigenvalue is $\exp(-2\pi \mathrm{i} k/L)$ and $2\pi k/L$ is the discrete lattice momentum. Here we made use of the fact that $T^L = 1$ (on a ring with L sites, L translations by one site let you return to the origin). This property also implies $\exp(-2\pi \mathrm{i} k) = 1$, hence k has to be an integer. Due to the periodicity of the exponential, we can restrict ourselves to $k = 0, 1, \ldots, (L-1)$.

The normalization of the state $P_k|n\rangle$ requires some care. We find

$$\begin{aligned} P_k^\dagger &= \frac{1}{L} \sum_{j=0}^{L-1} \mathrm{e}^{-2\pi \mathrm{i} jk/L} T^{-j} = \frac{1}{L} \sum_{j'=0}^{L-1} \mathrm{e}^{2\pi \mathrm{i} j'k/L} T^{j'} = P_k \\ P_k^2 &= \frac{1}{L^2} \sum_{i,j=0}^{L-1} \mathrm{e}^{2\pi \mathrm{i}(i-j)k/L} T^{i-j} = \frac{1}{L} \sum_{j'=0}^{L-1} \mathrm{e}^{2\pi \mathrm{i} j'k/L} T^{j'} = P_k \, , \end{aligned} \tag{18.16}$$

as we expect for a projector. Hence, $\langle n|P_k^\dagger P_k|n\rangle = \langle n|P_k^2|n\rangle = \langle n|P_k|n\rangle$. For most $|n\rangle$ the states $T^j|n\rangle$ with $j = 0, 1, \ldots, (L-1)$ will differ from each other, therefore $\langle n|P_k|n\rangle = 1/L$. However, some states are mapped onto themselves by a translation T^{ν_n} with $\nu_n < L$, i.e., $T^{\nu_n}|n\rangle = \mathrm{e}^{\mathrm{i}\phi_n}|n\rangle$ with a phase ϕ_n (usually 0 or

π). Nevertheless $T^L|n\rangle = |n\rangle$, therefore ν_n has to be a divider of L with $q_n = L/\nu_n$ an integer. Calculating the norm then gives

$$\langle n|P_k|n\rangle = \frac{1}{L}\sum_{j=0}^{q_n} \mathrm{e}^{\mathrm{i}(2\pi k/q_n+\phi_n)\,j} \;, \tag{18.17}$$

which equals $q_n/L = 1/\nu_n$ or 0 depending on k and ϕ_n.

How do the above ideas translate into a reduced dimension of our Hilbert space? Let us first consider the $\uparrow$-patterns from Table 18.1: All four patterns (states) are connected with a translation by one site, i.e., starting from the pattern $|0_\uparrow\rangle = 0111$ the other patterns are obtained through $|n_\uparrow\rangle = T^{-n}|0_\uparrow\rangle$,

$$\begin{aligned}
|0_\uparrow\rangle &= T^0|0_\uparrow\rangle = 0111 \;, \\
|1_\uparrow\rangle &= T^{-1}|0_\uparrow\rangle = 1011 \;, \\
|2_\uparrow\rangle &= T^{-2}|0_\uparrow\rangle = 1101 \;, \\
|3_\uparrow\rangle &= T^{-3}|0_\uparrow\rangle = 1110 \;.
\end{aligned} \tag{18.18}$$

We can call this group of connected states a cycle, which is completely described by knowing one of its members. It is convenient to use the pattern with the smallest integer value to be this special member of the cycle, and we call it the representative of the cycle.

Applying the projector to the representative of the cycle, $P_k|0_\uparrow\rangle$, we can generate L linearly independent states, which in our case reads

$$\begin{aligned}
P_0|0_\uparrow\rangle &= (0111 + 1011 + 1101 + 1110)/L \;, \\
P_1|0_\uparrow\rangle &= (0111 - \mathrm{i}\,1011 - 1101 + \mathrm{i}\,1110)/L \;, \\
P_2|0_\uparrow\rangle &= (0111 - 1011 + 1101 - 1110)/L \;, \\
P_3|0_\uparrow\rangle &= (0111 + \mathrm{i}\,1011 - 1101 - \mathrm{i}\,1110)/L \;.
\end{aligned} \tag{18.19}$$

The advantage of these new states, which are linear combinations of all members of the cycle in a spirit similar to discrete Fourier transformation, becomes clear when we apply the Hamiltonian: Whereas the Hamiltonian mixes the states in (18.18), all matrix elements between the states in (18.19) vanish. Hence, we have decomposed the four-dimensional Hilbert space into four one-dimensional blocks.

In a next step we repeat this procedure for the $\downarrow$-patterns of Table 18.1. These can be decomposed into two cycles represented by the states $|0_\downarrow\rangle = 0011$ and $|1_\downarrow\rangle = 0101$, where due to $T^2|1_\downarrow\rangle = -|1_\downarrow\rangle$ the second cycle has size $\nu_1 = 2$. Note, that we also have phase factors here, since the number of fermions is even. To get the complete symmetrized basis, we need to combine the up and down spin representatives, thereby taking into account relative shifts between the states. For our sample case the combined representatives,

$$|r\rangle = |n_\uparrow\rangle T^j |m_\downarrow\rangle \tag{18.20}$$

no.	patterns
0	0111×0011
1	0111×0110
2	0111×1100
3	0111×1001
4	0111×0101
5	0111×1010

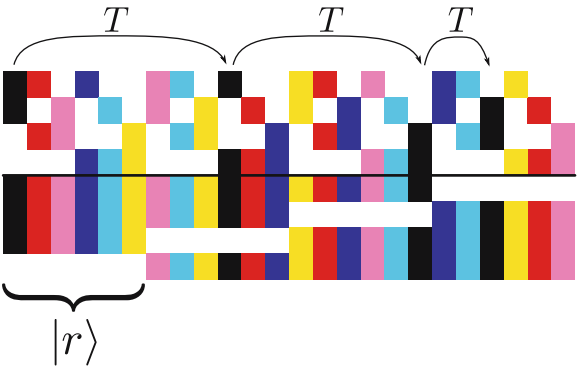

Fig. 18.3. Decomposition of the basis for $L = 4$, $N_\uparrow = 3$, $N_\downarrow = 2$ into six cycles

with $j = 0, 1, \ldots, \min(\nu_n, \nu_m) - 1$, are given in Fig. 18.3.

The basis of each of the L fixed-k (fixed-momentum) Hilbert spaces is then given by the states

$$|r_k\rangle = \frac{P_k|r\rangle}{\sqrt{\langle r|P_k|r\rangle}} \,, \tag{18.21}$$

where we discard those $|r\rangle$ with $\langle r|P_k|r\rangle = 0$. In our example all six states have $\langle r|P_k|r\rangle = 1/4\ \forall k$ and no state is discarded. Therefore the dimension of each fixed-k space is six, and summing over all four k we obtain the original number of states, 24. For other particle numbers or lattice sizes we may obtain representatives $|r\rangle$ with $\langle r|P_k|r\rangle = 0$ for certain k. An example is the case $N_\uparrow = N_\downarrow = 2$, $L = 4$ which leads to ten representatives, but two of them have $\langle r|P_k|r\rangle = 0$ for $k = 1$ and $k = 3$. Adding the dimensions of the four k-subspaces, we find $10+8+10+8 = 36$, which agrees with $\binom{L}{N_\downarrow}\binom{L}{N_\uparrow} = 6^2$.

When calculating the Hamiltonian matrix for a given k-sector, we can make use of the fact that H commutes with T, and therefore also with P_k. Namely, the matrix element between two states $|r_k\rangle$ and $|r'_k\rangle$ is simply given by

$$\langle r'_k|H|r_k\rangle = \frac{\langle r'|P_k H P_k|r\rangle}{\sqrt{\langle r'|P_k|r'\rangle\langle r|P_k|r\rangle}} = \frac{\langle r'|P_k H|r\rangle}{\sqrt{\langle r'|P_k|r'\rangle\langle r|P_k|r\rangle}} \,, \tag{18.22}$$

i.e., we need to apply the projector only once after we applied H to the representative $|r\rangle$. Repeating the procedure for all representatives, we obtain the matrix for a given k. The full matrix with fixed particle numbers $N_\uparrow$ and $N_\downarrow$ is decomposed into L blocks with fixed k. For example, the 24×24 matrix from Fig. 18.2 is decomposed into the four 6×6 matrices.

$$H_{k=0} = \begin{pmatrix} 2U & -t & -t & t & t & 0 \\ -t & 2U & -t & -t & 0 & t \\ -t & -t & 2U & 0 & -t & -t \\ t & -t & 0 & U & -t & t \\ t & 0 & -t & -t & U & -t \\ 0 & t & -t & t & -t & U \end{pmatrix} \quad H_{k=1} = \begin{pmatrix} 2U & -t & -\mathrm{i}t & -\mathrm{i}t & t & 0 \\ -t & 2U & -t & -t & -2\mathrm{i}t & t \\ \mathrm{i}t & -t & 2U & 0 & -t & -\mathrm{i}t \\ \mathrm{i}t & -t & 0 & U & -t & -\mathrm{i}t \\ t & 2\mathrm{i}t & -t & -t & U & -t \\ 0 & t & \mathrm{i}t & \mathrm{i}t & -t & U \end{pmatrix}$$

$$H_{k=2} = \begin{pmatrix} 2U & -t & t & -t & t & 0 \\ -t & 2U & -t & -t & 0 & t \\ t & -t & 2U & 0 & -t & t \\ -t & -t & 0 & U & -t & -t \\ t & 0 & -t & -t & U & -t \\ 0 & t & t & -t & -t & U \end{pmatrix} \quad H_{k=3} = \begin{pmatrix} 2U & -t & \mathrm{i}t & \mathrm{i}t & t & 0 \\ -t & 2U & -t & -t & 2\mathrm{i}t & t \\ -\mathrm{i}t & -t & 2U & 0 & -t & \mathrm{i}t \\ -\mathrm{i}t & -t & 0 & U & -t & \mathrm{i}t \\ t & -2\mathrm{i}t & -t & -t & U & -t \\ 0 & t & -\mathrm{i}t & -\mathrm{i}t & -t & U \end{pmatrix} \tag{18.23}$$

Note that except for $k = 0$ and $k = 2$, which correspond to the momenta zero and π, the matrices H_k are complex. Their dimension, however, is a factor of L smaller than the dimension of the initial space with fixed particle numbers. At first glance, the above matrices look rather dense. This is due to the small dimension of our sample system. For larger L and N_e the Hamiltonian is as sparse as the example of Fig. 18.1.

18.1.6 A few Remarks about Spin Systems

We mentioned earlier that the Heisenberg model (18.2) can be derived from the Hubbard model (18.1) considering the limit $U \to \infty$. Consequently, the numerical setup for both models is very similar. For a model with $|\boldsymbol{S}_i| = 1/2$, we can choose the z-axis as the quantization axis and encode the two possible spin directions $\downarrow$ and $\uparrow$ into the bit values zero and one, e.g., $\downarrow\uparrow\downarrow\downarrow\rightarrow 0100$. If applicable, the conservation of the total spin $S^z = \sum_i S_i^z$ is similar to a particle number conservation, i.e., we can easily construct all basis states with fixed S^z using the ideas described earlier. The same holds for translational invariance, where now the construction of a symmetric basis is made easier by the lack of fermionic phase factors (spin operators at different sites commute). When calculating matrix elements it is convenient to rewrite the exchange interaction as

$$\boldsymbol{S}_i \boldsymbol{S}_j = \frac{1}{2}\left(S_i^+ S_j^- + S_i^- S_j^+\right) + S_i^z S_j^z \;, \tag{18.24}$$

where the operators $S_i^\pm = S_i^x \pm \mathrm{i} S_i^y$ rise or lower the S_i^z value at site i, which is easy to implement in our representation. Note also, that from this equation the conservation of the total S^z is obvious.

If the considered solid consists of more complex ions with partially filled shells, we may also arrive at Heisenberg type models with $|\boldsymbol{S}_i| > 1/2$. In this case we need $2|\boldsymbol{S}_i| + 1$ states per site to describe all possible S^z-orientations and, of course, this requires more than one bit per site. Numbering all possible states with a given total S^z is slightly more complicated. For instance, we can proceed recursively adding one site at each time.

18.1.7 Phonon Systems

Having constructed a symmetrized basis for the Hubbard and Heisenberg type models, let us now comment on bosonic models and phonons, in particular. For such systems the particle number is usually not conserved, and the accessible Hilbert space is infinite even for a single site. For numerical studies we therefore need an appropriate truncation scheme, which preserves enough of the Hilbert space to describe the considered physics, but restricts the dimension to manageable values. Assume we are studying a model like the Holstein-Hubbard model (18.3), where the pure phonon part is described by a set of harmonic Einstein oscillators, one at each site. For an L-site lattice the eigenstates of this phonon system are given by the Fock states

$$|m_0,\ldots,m_{L-1}\rangle = \prod_{i=0}^{L-1} \frac{(b_i^\dagger)^{m_i}}{\sqrt{m_i!}}|0\rangle \tag{18.25}$$

and the corresponding eigenvalue is

$$E_\mathrm{p} = \omega_0 \sum_{i=0}^{L-1} m_i \ . \tag{18.26}$$

If we are interested in the ground state or the low energy properties of the interacting electron-phonon model (18.3), certainly only phonon states with a rather low energy will contribute. Therefore, a good truncated basis for the phonon Hilbert space is given by the states

$$|m_0,\ldots,m_{L-1}\rangle \quad \text{with} \quad \sum_{i=0}^{L-1} m_i \leq M \ , \tag{18.27}$$

which include all states with $E_\mathrm{p} \leq \omega_0 M$. The dimension of the resulting Hilbert space is $\binom{L+M}{M}$.

To keep the required M small, we apply another trick [7]. After Fourier transforming the phonon subsystem,

$$b_i = \frac{1}{\sqrt{L}} \sum_{k=0}^{L-1} \mathrm{e}^{2\pi \mathrm{i} i k/L} \widetilde{b}_k \ , \tag{18.28}$$

we observe that the phonon mode with $k = 0$ couples to a conserved quantity: The total number of electrons N_e,

$$\begin{aligned} H = &-t \sum_{\langle ij\rangle,\sigma} (c_{i\sigma}^\dagger c_{j\sigma} + \text{H.c.}) + U \sum_i n_{i\uparrow} n_{i\downarrow} + \omega_0 \sum_k \widetilde{b}_k^\dagger \widetilde{b}_k \\ &- \frac{g\omega_0}{\sqrt{L}} \sum_{i,\sigma} \sum_{k\neq 0} \mathrm{e}^{-2\pi \mathrm{i} i k/L} (\widetilde{b}_k^\dagger + \widetilde{b}_{-k}) n_{i\sigma} - \frac{g\omega_0}{\sqrt{L}} (\widetilde{b}_0^\dagger + \widetilde{b}_0) N_\mathrm{e} \ . \end{aligned} \tag{18.29}$$

With a constant shift $\widetilde{b}_0 = \widehat{b}_0 + gN_\mathrm{e}/\sqrt{L}$ this part of the model can thus be solved analytically. Going back to real space and using the equivalently shifted phonons $b_i = \bar{b}_i + gN_\mathrm{e}/L$, the transformed Hamiltonian reads

$$H = -t \sum_{\langle ij\rangle,\sigma} (c^\dagger_{i\sigma} c_{j\sigma} + \text{H.c.}) + U \sum_i n_{i\uparrow} n_{i\downarrow} + \omega_0 \sum_i \bar{b}^\dagger_i \bar{b}_i$$
$$-g\omega_0 \sum_i (\bar{b}^\dagger_i + \bar{b}_i)(n_{i\uparrow} + n_{i\downarrow} - N_\mathrm{e}/L) - \omega_0 (gN_\mathrm{e})^2/L \,. \quad (18.30)$$

Since the shifted phonons $\bar{b}^{(\dagger)}_i$ couple only to the local charge fluctuations, in a simulation the same accuracy can be achieved with a much smaller cutoff M, compared to the original phonons $b^{(\dagger)}_i$. This is particularly important in the case of strong interaction g.

As in the electronic case, we can further reduce the basis dimension using the translational symmetry of our lattice model. Under periodic boundary conditions, the translation operator T transforms a given basis state like

$$T|m_0, \ldots, m_{L-1}\rangle = |m_{L-1}, m_0, \ldots, m_{L-2}\rangle \,. \quad (18.31)$$

Since we are working with bosons, no additional phase factors can occur, and everything is a bit easier. As before, we need to find the representatives $|r_\mathrm{p}\rangle$ of the cycles generated by T, and then construct eigenstates of T with the help of the projection operator P_k. When combining the electronic representatives $|r_\mathrm{e}\rangle$ from (18.20) with the phonon representatives $|r_\mathrm{p}\rangle$, we proceed in the same way, as we did for the up and down spin channels, $|r\rangle = |r_\mathrm{e}\rangle T^j |r_\mathrm{p}\rangle$. A full symmetrized basis state of the interacting electron-phonon model is then given by $P_k|r\rangle$. Note that the product structure of the electron-phonon basis is preserved during symmetrization, which is a big advantage for parallel implementations [8].

Having explained the construction of a symmetrized basis and of the corresponding Hamiltonian matrix for both electron and phonon systems, we are now ready to work with these matrices. In particular, we will show how to calculate eigenstates and dynamic correlations of our physical systems.

18.2 Eigenstates of Sparse Matrices

18.2.1 The Lanczos Algorithm

The Lanczos algorithm is one of the simplest methods for the calculation of extremal (smallest or largest) eigenvalues of sparse matrices [9]. Initially it was developed for the tridiagonalization of Hermitian matrices [10], but it turned out, not to be particularly successful for this purpose. The reason for its failure as a tridiagonalization algorithm is the underlying recursion procedure, which rapidly converges to eigenstates of the matrix and therefore looses the orthogonality between subsequent vectors that is required for tridiagonalization. Sometimes, however, deficiencies turn into advantages, and the Lanczos algorithm made a successful career as an eigenvalue solver.

The basic structure and the implementation of the algorithm is very simple. Starting from a random initial state (vector) $|\phi_0\rangle$, we construct the series of states

$H^n|\phi_0\rangle$ by repeatedly applying the matrix H (i.e., the Hamiltonian). This series of states spans what is called a Krylov space in the mathematical literature, and the Lanczos algorithm therefore belongs to a broader class of algorithms that work on Krylov spaces [11]. Next we orthogonalize these states against each other to obtain a basis of the Krylov space. Expressed in terms of this basis, the matrix turns out to be tridiagonal. We can easily perform these two steps in parallel, and obtain the following recursion relation:

$$\begin{aligned} |\phi'\rangle &= H|\phi_n\rangle - \beta_n|\phi_{n-1}\rangle \;, \\ \alpha_n &= \langle\phi_n|\phi'\rangle \;, \\ |\phi''\rangle &= |\phi'\rangle - \alpha_n|\phi_n\rangle \;, \\ \beta_{n+1} &= ||\phi''|| = \sqrt{\langle\phi''|\phi''\rangle} \;, \\ |\phi_{n+1}\rangle &= |\phi''\rangle/\beta_{n+1} \;, \end{aligned} \tag{18.32}$$

where $|\phi_{-1}\rangle = 0$ and $|\phi_0\rangle$ is a random normalized state, $||\phi_0|| = 1$.

The coefficients α_n and β_n form the tridiagonal matrix, which we are looking for,

$$\widetilde{H}_N = \begin{pmatrix} \alpha_0 & \beta_1 & 0 & \cdots\cdots & 0 \\ \beta_1 & \alpha_1 & \beta_2 & 0 \quad \cdots & 0 \\ 0 & \beta_2 & \alpha_2 & \beta_3 \quad 0 & 0 \\ & & \ddots & \ddots \quad \ddots & \\ 0 & \cdots & 0 & \beta_{N-2} \; \alpha_{N-2} & \beta_{N-1} \\ 0 & \cdots & 0 & \beta_{N-1} \; \alpha_{N-1} & \end{pmatrix} . \tag{18.33}$$

With increasing recursion order N the eigenvalues of $\widetilde{H}_N$ – starting with the extremal ones – converge to the eigenvalues of the original matrix H. In Fig. 18.4 we illustrate this for the ground-state energy of the one-dimensional Hubbard model (18.1) on a ring of 12 and 14 sites. Using only particle number conservation, the corresponding matrix dimensions are $D = \binom{12}{6}^2 = 853776$ and $D = \binom{14}{7}^2 = 11778624$, respectively. With about 90 iterations the precision of the lowest eigenvalue is better than 10^{-13}, where we compare with the exact result obtained with Bethe ansatz [4]. The eigenvalues of the tridiagonal matrix were calculated with standard library functions from the LAPACK collection [12]. Since $N \ll D$, this accounts only for a tiny fraction of the total computation time, which is governed by the application of H on $|\phi_n\rangle$.

Having found the extremal eigenvalues, we can also calculate the corresponding eigenvectors of the matrix. If the eigenvector $|\psi\rangle$ of the tridiagonal matrix $\widetilde{H}_N$ has the components ψ_j, i.e., $|\psi\rangle = \{\psi_0, \psi_1, \ldots, \psi_{N-1}\}$, the eigenvector $|\Psi\rangle$ of the original matrix H is given by

$$|\Psi\rangle = \sum_{j=0}^{N-1} \psi_j |\phi_j\rangle \;. \tag{18.34}$$

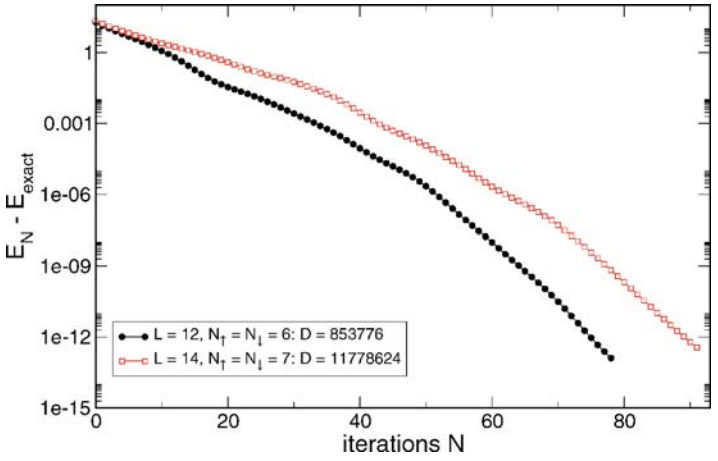

Fig. 18.4. Convergence of the Lanczos recursion for the ground-state energy of the Hubbard model on a ring of $L = 12$ and $L = 14$ sites

To calculate this sum we simply need to repeat the above Lanczos recursion with the same start vector $|\phi_0\rangle$, thereby omitting the scalar products for α_j and β_j, which we know already.

The efficiency of the Lanczos algorithm is based on three main properties:

(i) It relies only on matrix vector multiplications (MVM) of the matrix H with a certain vector $|\phi_n\rangle$. If H is sparse, this requires only of the order of D operations, where D is the dimension of H.

(ii) When calculating eigenvalues, the algorithm requires memory only for two vectors of dimension D and for the matrix H. For exceptionally large problems, the matrix can be re-constructed on-the-fly for each MVM, and the memory consumption is determined by the vectors. When calculating eigenvectors we need extra memory.

(iii) The first few eigenvalues on the upper and lower end of the spectrum of H usually converge very quickly. In most cases $N \lesssim 100$ iterations are sufficient.

Extensions of the Lanczos algorithm can also be used for calculating precise estimates of the full spectral density of H, or of dynamical correlation functions that depend on the spectrum of H and on the measured operators. We will discuss more details in Chap. 19 when we describe Chebyshev expansion based methods, such as the Kernel Polynomial Method.

18.2.2 The Jacobi-Davidson Algorithm

The Jacobi-Davidson method is a recent, more involved approach to the sparse eigenvalue problem, which was suggested by Sleijpen and van der Vorst [13] as a combination of Davidson's method [14] and a procedure described by Jacobi [15].

It has the advantage that not only the lowest eigenstates but also excitations converge rapidly. In addition, it can correctly resolve degeneracies.

In the Jacobi-Davidson algorithm, like in the Lanczos algorithm, a set of vectors $V_N = \{|v_0\rangle, \ldots, |v_{N-1}\rangle\}$ is constructed iteratively, and the eigenvalue problem for the Hamiltonian H is solved within this subspace. However, in contrast to the Lanczos algorithm, we do not work in the Krylov space of H, but instead expand V_N with a vector that is orthogonal to our current approximate eigenstates. In more detail, the procedure is as follows:

(i) Initialize the set V with a random normalized start vector, $V_1 = \{|v_0\rangle\}$.
(ii) Compute all unknown matrix elements $\langle v_i|H|v_j\rangle$ of $\widetilde{H}_N$ with $|v_i\rangle \in V_N$.
(iii) Compute an eigenstate $|s\rangle$ of $\widetilde{H}_N$ with eigenvalue θ, and express $|s\rangle$ in the original basis, $|u\rangle = \sum_i |v_i\rangle\langle v_i|s\rangle$.
(iv) Compute the associated residual vector $|r\rangle = (H-\theta)|u\rangle$ and stop the iteration, if its norm is sufficiently small.
(v) Otherwise, (approximately) solve the linear equation

$$(1 - |u\rangle\langle u|)(H - \theta)(1 - |u\rangle\langle u|)|t\rangle = -|r\rangle\,. \tag{18.35}$$

(vi) Orthogonalize $|t\rangle$ against V_N with the modified Gram-Schmidt method and append the resulting vector $|v_N\rangle$ to V_N, obtaining the set V_{N+1}.
(vii) Return to step (ii).

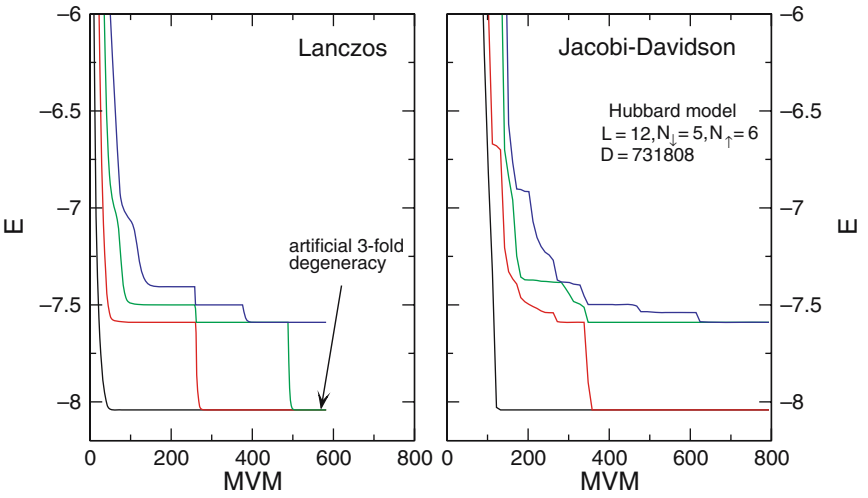

Fig. 18.5. Comparison of the Jacobi-Davidson algorithm and the Lanczos algorithm applied to the four lowest eigenstates of the Hubbard model with $L = 12$, $N_\downarrow = 5$, $N_\uparrow = 6$. Jacobi-Davidson correctly resolves the two-fold degeneracy, standard Lanczos (although faster) cannot distinguish true and artificial degeneracy

For (18.35) we only need an approximate solution, which can be obtained, for instance, with a few steps of the Generalized Minimum Residual Method (GMRES) or the Quasi Minimum Residual Method (QMR) [16]. If more than one eigenstate is desired, the projection operator $(1 - |u\rangle\langle u|)$ needs to be extended by the already converged eigenstates, $(1 - \sum_k |u_k\rangle\langle u_k|)$, such that the search continues in a new, yet unexplored direction. Since the Jacobi-Davidson algorithm requires memory for all the vectors in V_N, it is advisable to restart the calculation after a certain number of steps. There are clever strategies for this restart, and also for the calculation of interior eigenstates, which are hard to access with Lanczos. More details can be found in the original papers [13, 17] or in text books [18].

In Fig. 18.5 we give a comparison of the Lanczos and the Jacobi-Davidson algorithms, calculating the four lowest eigenstates of the Hubbard model on a ring of $L = 12$ sites with $N_\downarrow = 5$ and $N_\uparrow = 6$ electrons. The matrix dimension is $D = 731808$, and each of the lowest states is two-fold degenerate. In terms of speed and memory consumption the Lanczos algorithm has a clear advantage, but with the standard setup we have difficulties resolving the degeneracy. The method tends to create artificial copies of well converged eigenstates, which are indistinguishable from the true degenerate states. The problem can be circumvented with more advanced variants of the algorithm, such as Block or Band Lanczos [9, 18], but we loose the simplicity of the method and part of its speed. Jacobi-Davidson then is a strong competitor. It is not much slower and it correctly detects the two-fold degeneracy, since the converged eigenstates are explicitly projected out of the search space.

References

1. J. Hubbard, Proc. Roy. Soc. London, Ser. A **276**, 238 (1963) 529
2. M.C. Gutzwiller, Phys. Rev. Lett. **10**, 159 (1963) 529
3. J. Kanamori, Prog. Theor. Phys. **30**, 275 (1963) 529
4. E.H. Lieb, F.Y. Wu, Phys. Rev. Lett. **20**, 1445 (1968) 529, 540
5. F.H.L. Essler, H. Frahm, F. Göhmann, A. Klümper, V.E. Korepin, *The One-Dimensional Hubbard Model* (Cambridge University Press, Cambridge, 2005) 529
6. R. Sedgewick, *Algorithmen* (Addison-Wesley, Bonn, 1992) 533
7. S. Sykora, A. Hübsch, K.W. Becker, G. Wellein, H. Fehske, Phys. Rev. B **71**, 045112 (2005) 538
8. B. Bäuml, G. Wellein, H. Fehske, Phys. Rev. B **58**, 3663 (1998) 539
9. J.K. Cullum, R.A. Willoughby, *Lanczos Algorithms for Large Symmetric Eigenvalue Computations*, vol. I & II (Birkhäuser, Boston, 1985) 539, 543
10. C. Lanczos, J. Res. Nat. Bur. Stand. **45**, 255 (1950) 539
11. Y. Saad, *Numerical Methods for Large Eigenvalue Problems* (University Press, Manchester, 1992). URL `http://www-users.cs.umn.edu/ saad/books.html` 540
12. Linear Algebra PACKage. URL `http://www.netlib.org` 540
13. G.L.G. Sleijpen, H.A. van der Vorst, SIAM J. Matrix Anal. Appl. **17**, 401 (1996) 541, 543
14. E.R. Davidson, J. Comput. Phys. **17**, 87 (1975) 541
15. C.G.J. Jacobi, J. Reine und Angew. Math. **30**, 51 (1846) 541

16. Y. Saad, *Iterative Methods for Sparse Linear Systems*, 2nd edn. (SIAM, Philadelphia, 2003). URL http://www-users.cs.umn.edu/ saad/books.html 543
17. D.R. Fokkema, G.L.G. Sleijpen, H.A. van der Vorst, SIAM J. Sci. Comp. **20**, 94 (1998) 543
18. Z. Bai, J. Demmel, J. Dongarra, A. Ruhe, H. van der Vorst (eds.), *Templates for the Solution of Algebraic Eigenvalue Problems: A Practical Guide* (SIAM, Philadelphia, 2000). URL http://www.cs.utk.edu/ dongarra/etemplates/ 543